Title

Patterning All-Inorganic Halide Perovskite with Adjustable Phase for High-Resolution Color Filter and Photodetector Arrays

Journal

Advanced Functional Materials, 32(16)

ISSN

1616-301X

Authors

Kim, Woosik
Kim, Su-Kyung
Jeon, Sanghyun
et al.

Publication Date

2022-04-01

DOI

10.1002/adfm.202111409

Peer reviewed

ADVANCED FUNCTIONAL MATERIALS
www.afm-journal.de

Patterning All-Inorganic Halide Perovskite with Adjustable Phase for High-Resolution Color Filter and Photodetector Arrays

*Woosik Kim, Su-Kyung Kim, Sanghyun Jeon, Junhyuk Ahn, Byung Ku Jung, Sang Yeop Lee, Chanho Shin, Tae-Yeon Seong, Sohee Jeong, Ho Seong Jang, TSe Nga Ng, and Soong Ju Oh**

Perovskite has been actively studied for optoelectronic applications, such as photodetectors and light-emitting diodes (LEDs), because of its excellent optoelectronic properties. However, ionic bonds of the perovskite structure are vulnerable to chemicals, which makes perovskite incompatible with photolithography processes that use polar solvents. Such incompatibility with photolithography hinders perovskite patterning and device integration. Here, an all-solution based cesium lead halide perovskite ($Cs_xPb_yBr_z$) patterning method is introduced in which $PbBr_2$ is patterned and then synthesized into $Cs_xPb_yBr_z$. Each step of the top-down patterning process (e.g., developing, etching, and rinsing) is designed to be compatible with existing photolithography equipment. Structural, chemical, and optical analyses show that the $PbBr_2$ pattern of $(10\ \mu m)^2$ squares is successfully transformed into $CsPbBr_3$ and Cs_4PbBr_6 with excellent absorption and emission properties. High-resolution photoconductor arrays and luminescent pattern arrays are fabricated with $CsPbBr_3$ and Cs_4PbBr_6 on various substrates, including flexible plastic films, to demonstrate their potential applications in image sensors or displays. The research provides a fundamental understanding of the properties and growth of perovskite and promotes technological advancement by preventing degradation during the photolithography process, enabling the integration of perovskite arrays into image sensors and displays.

1. Introduction

Lead halide perovskites are known for their excellent optical and optoelectronic properties, such as high light absorption coefficient, narrow full width at half maximum, and adjustable bandgap.[1–3] These materials are also readily synthesized on a large scale via solution processing.[4–6] These advantages have led to the research and fabrication of high-performance optoelectronic devices such as light-emitting diodes (LEDs),[7–10] photodetectors,[11–13] and photovoltaic cells[14–17] with high efficiency. To integrate a single device into a display or sensor system, it must be patterned and developed into device arrays.[18] The patterning process is a critical step toward industrial fabrication to scale up and integrate components in high density for color filters, display arrays, and image sensors.

Top-down lithography is widely used in research and industry for the pattern production of optical and optoelectronic devices because it is fast, highly reproducible, and enables high-resolution patterning of large areas. However, lead halide perovskite materials cannot be directly placed in conventional top-down lithography because of their ionic bonding properties. For example, when perovskites are exposed to polar solvents such as photoresist (PR) and developers used in photolithography, degradation in optical and optoelectronic properties is observed due to ionization dissolution. This means that the existing top-down lithography process is not suitable for patterning perovskite materials. Therefore, patterning is one of the major obstacles to scale up perovskite-based optoelectronic device systems.

Various studies have been conducted aimed at high-resolution patterning by conventional lithography processes while maintaining the superior properties of perovskite. For example, polymers have been used as a protective layer to prevent the degradation of perovskite by keeping it from being exposed to the solvent during lithography.[19,20] Another method involving patterning a hydrophobic self-assembled monolayer, in which the perovskite was selectively grown according to the

W. Kim, S.-K. Kim, S. Jeon, J. Ahn, B. K. Jung, S. Y. Lee, T.-Y. Seong, S. J. Oh
Department of Materials Science and Engineering
Korea University
Seoul 02841, South Korea
E-mail: sjoh1982@korea.ac.kr

C. Shin, T. N. Ng
Materials Science Engineering Program and Department of Electrical and Computer Engineering
University of California San Diego
La Jolla, CA 92093, USA

S. Jeong, H. S. Jang
Materials Architecturing Research Center
Korea Institute of Science and Technology (KIST)
Seoul 02792, Republic of Korea

The ORCID identification number(s) for the author(s) of this article can be found under https://doi.org/10.1002/adfm.202111409.

DOI: 10.1002/adfm.202111409

monolayer template patterned on the substrate to prevent exposure to etching solvents.[21–24] However, since these methods require gas or plasma etching, high-energy light emissions, and chemical vapor deposition, those multiple high-cost processes are not amendable for commercialization. A new perovskite patterning technique with high-resolution, compatible with conventional lithography and applicable to various perovskite materials or structures is needed.

In this study, we demonstrate an all-solution processed patterning technique using two-step perovskite fabrication. Instead of using cesium lead bromide ($Cs_xPb_yBr_z$), which is vulnerable to the lithography process, a patterning strategy for $PbBr_2$ is introduced and subsequently the $PbBr_2$ is transformsed into $Cs_xPb_yBr_z$ via CsBr solution-phase deposition. Process with simultaneous development and etching (SDE) and termination reaction assisted by *iso*-propyl alcohol (IPA) were developed, resulting in high-resolution $PbBr_2$ patterns that maintained their shapes during transformation to $Cs_xPb_yBr_z$. The structural and phase changes from the reaction were analyzed by optical, chemical, and structural characterization. The resolution of the fabricated $Cs_xPb_yBr_z$ perovskite pattern reached 10 µm. By converting it into two types of perovskites with different optical properties according to the reaction time, we successfully implemented a luminescent array and a photodetector array. Our method integrates the development and etching processes into the existing photolithography process to produce a high-resolution perovskite pattern with controllable phases and properties without complex expensive procedures while utilizing commonly used materials. This method will be applicable in the fabrication of perovskite optoelectronic device arrays such as LED displays and image sensors.

2. Results and Discussion

Figure 1a shows the two-step patterning process of the $Cs_xPb_yBr_z$. As perovskite is degraded by chemicals used in photolithography, we applied lithography to pattern $PbBr_2$ films instead of fully synthesized $Cs_xPb_yBr_z$ films. Then, $PbBr_2$ was transformed into $Cs_xPb_yBr_z$. Briefly, the $PbBr_2$ film was deposited by spin-coating a $PbBr_2$ solution (1 M in dimethylformamide (DMF)) on a substrate, followed by annealing at 90 °C for 60 min. Then, the PR was spin-coated and selectively exposed to 365 nm UV light through a photomask. The $PbBr_2$ pattern was formed by the SDE process using tetramethylammonium hydroxide (TMAH) and deionized water (DI), which simultaneously developed the PR and etched the $PbBr_2$ film (Figure 1b). The patterned $PbBr_2$ film was then dipped into CsBr solution to transform it into $Cs_xPb_yBr_z$ (Figure 1c). After the reaction, the residual CsBr was removed by an IPA-assisted reaction

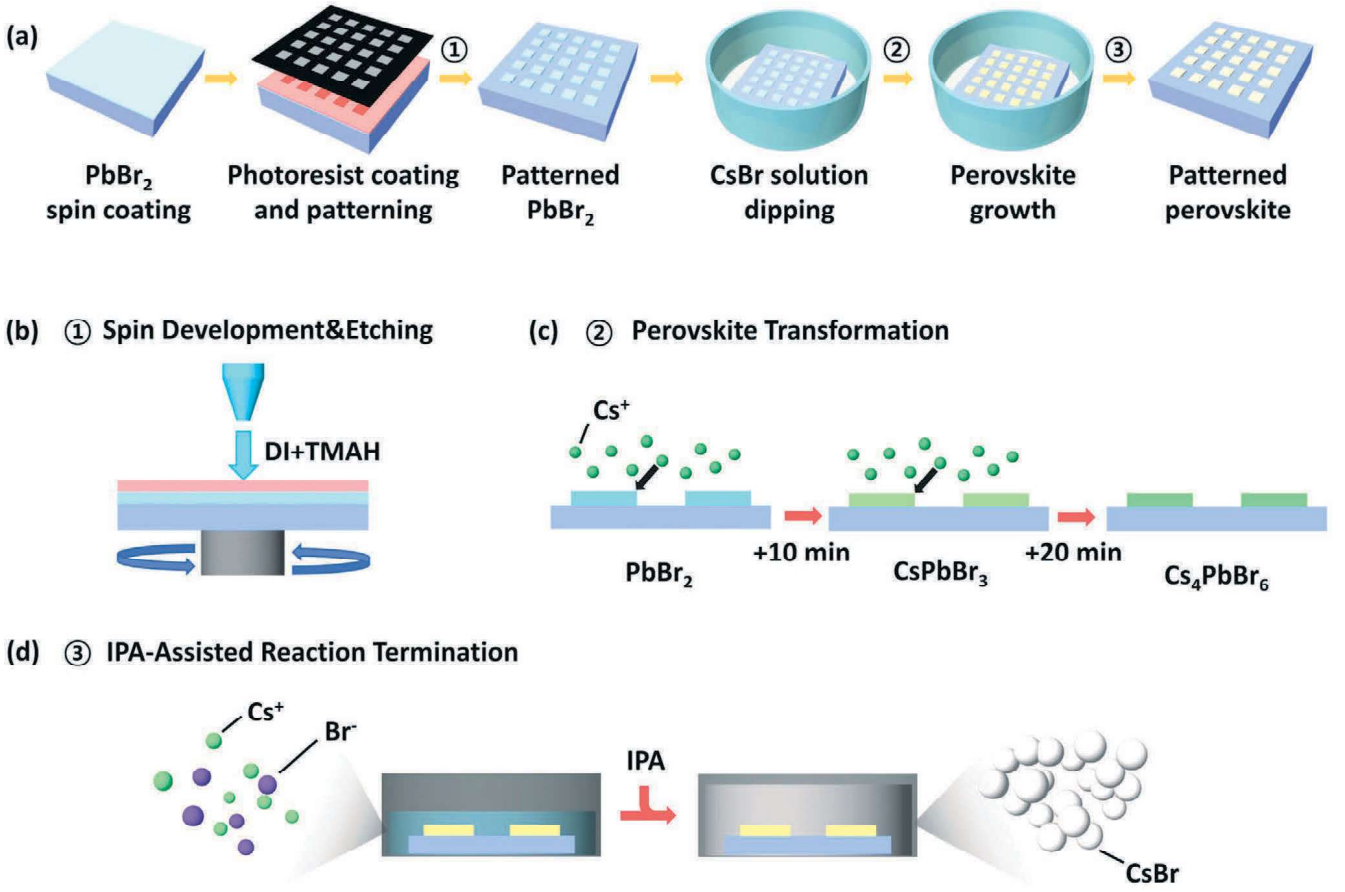

Figure 1. a) Schematic illustration of the $PbBr_2$ patterning and perovskite transformation process. b) SDE method, c) perovskite transformation, and d) IPA-assisted reaction termination.

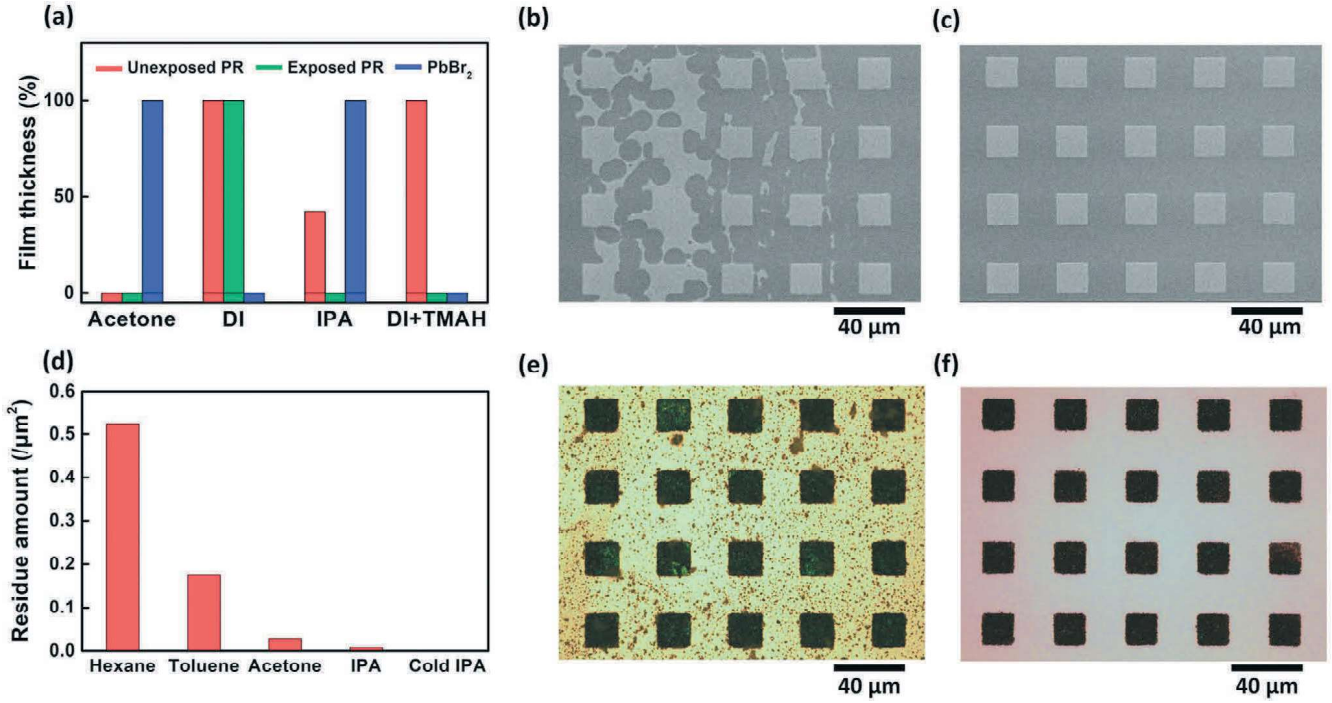

Figure 2. a) Film thickness after solvent treatment of the PR and $PbBr_2$ film. SEM images of $PbBr_2$ patterns fabricated by SDE with b) immersion and c) spinning. d) Amount of residues in the perovskite pattern by solvents. Optical microscope images of the perovskite pattern rinsed by e) hexane and f) −20 °C IPA (scale bar = 40 μm).

termination method, followed by rinsing and annealing to produce the $Cs_xPb_yBr_z$ patterns (Figure 1d).

To develop an efficient lithographic process, we established an SDE process. In the top-down lithography process, SDE increased efficiency and reduced the process steps and costs. The solvent used for SDE must be able to etch $PbBr_2$ and have PR selectivity by removing only the UV-exposed PR. To meet these requirements, the PR selectivity and $PbBr_2$ etching ability were investigated with various solvents (**Figure 2**a; Figure S1, Supporting Information). The $PbBr_2$ etching ability and PR selectivity were evaluated by monitoring the change in film thickness after solvent treatment. The rate of remaining film thickness after treatment is compared in Figure 2a, respectively. Acetone and IPA did not react with $PbBr_2$; hence, they did not have $PbBr_2$ etching ability. DI completely removed $PbBr_2$ and showed a high etching ability. PR selectivity was evaluated by observing the change in the film thickness of the UV-exposed and unexposed PR after solvent treatment. Acetone dissolved the PR regardless of UV exposure, while DI did not; hence, neither solvent has PR selectivity. IPA completely dissolved the UV-exposed PR and partially dissolved the unexposed PR; hence, it has low PR selectivity. However, IPA cannot etch $PbBr_2$. It is well known that adding TMAH to DI results in PR selectivity; we found that TMAH addition had no effect on the $PbBr_2$ etching ability of DI. The TMAH aqueous solution has both the highest PR selectivity and $PbBr_2$ etching ability; hence, it is suitable as a solvent for the SDE process.

As the PR and $PbBr_2$ film were successfully developed and etched by the TMAH aqueous solution, the SDE process was conducted by immersing the patterned PR/$PbBr_2$ film in the TMAH aqueous solution. As seen in Figure 2b, a pattern was formed along with residues owing to the difference between the removal rates of PR and $PbBr_2$ film. The PR took ≈15 s to develop by TMAH aqueous solution, while the $PbBr_2$ film was etched immediately upon exposure to the solution. If the PR fails to develop uniformly, then there is a time difference from when $PbBr_2$ was exposed to the solution. If some regions are overexposed to the solution, the solution penetrates the PR pattern and overetching of the $PbBr_2$ pattern occurs. Conversely, when a certain area is exposed to the solution for less than the required time, the PR insufficiently develops and results in an unetched region. Thus, it is important to control the solution exposure time for smaller and finer patterns. However, it is very difficult to control the processing time with the immersion method because the aqueous solution has a nonuniform flow, resulting in a nonuniform pattern.

To resolve this issue, we developed a spin-SDE method that creates a uniform flow of the aqueous TMAH solution. In this method, the solution is introduced into the substrate as it spins. The spinning generates a centrifugal force, resulting in a uniform solution flow from the center to the edge of the substrate. In this way, when the solvent completes the SDE by reacting with the PR and $PbBr_2$ on the substrate, it is rapidly discharged to the edge and a new solvent is added to the center; thus, the SDE is conducted uniformly across the entire surface by the solvent at a uniform concentration. The $PbBr_2$ pattern produced using the spin-SDE method has higher uniformity and repeatability compared with the conventional immersion method (Figure 2c).

The patterned $PbBr_2$ film can be chemically transformed into $Cs_xPb_yBr_z$ through immersion in CsBr solution (Figure S2, Supporting Information). In the ternary Cs-Pb-Br system, there

are typically three phases: $CsPb_2Br_5$, $CsPbBr_3$, and Cs_4PbBr_6, according to the ratio of each element.[25] Bulk $CsPbBr_3$ is known to have excellent light absorption performance, while bulk Cs_4PbBr_6 exhibits excellent luminescence performance.[26] By controlling the reaction conditions (time and concentration), $CsPbBr_3$ and Cs_4PbBr_6 are synthesized. $CsPbBr_3$ was synthesized by immersion in CsBr solution for 10 min. Cs_4PbBr_6 was synthesized by immersion for a longer period (30 min) to increase Cs diffusion because of its higher Cs content.

When the reaction was completed, a perovskite pattern was formed, but a large amount of residue remained. Because the CsBr solution was almost saturated and evaporated quickly at 50 °C because of the high vapor pressure of methanol, CsBr crystals start to precipitate when the substrate is taken out of the solution. Therefore, there were many impurities near the pattern edges after $Cs_xPb_yBr_z$ was synthesized. To solve this problem, we designed an efficient perovskite rinsing process by examining the properties of solvents.

In the rinsing method, CsBr was precipitated in the solution instead of directly precipitated on the substrate. This was achieved by adding a rinsing solvent to the solution containing the substrate, and the substrate was rinsed while being taken out of the solution. The rinsing solvent must satisfy following conditions to prevent residue formation and the degradation of $Cs_xPb_yBr_z$ patterns: i) it should not degrade perovskite; ii) it should be poor solvent for CsBr to precipitate it; and iii) it should not leave residue on the substrate after rinsing. Hexane, toluene, acetone, and IPA were prepared, which are known to be solvents that are not damaging to perovskites. As all four solvents showed negligible dissolution of CsBr, the amount of residue after rinsing was compared (Figure 2d). After rinsing, the amount of residue was highest using hexane. For the remaining solvents, the amount of residue decreased in order of toluene, acetone, and IPA (Figure 2e,f; Figure S3, Supporting Information). Thus, IPA was chosen as the rinsing solvent because of its proper solubility and excellent rinsing performance without damaging perovskite properties (Figure S4, Supporting Information).[27–30]

IPA produced the least amount of residue, but did not completely clean areas between structures. To prevent CsBr from precipitating on the substrate, we designed an environment in which CsBr can be completely removed in solution. −20 °C IPA was used to decrease the solubility of CsBr in its solution and facilitate the precipitation. By adding −20 °C IPA, CsBr was instantaneously precipitated in the solution and the remaining residue was removed by rinsing to obtain clean patterns (See discussions in Supporting Information and Figure S3e in the Supporting Information).

Figure 3 shows the structural analysis conducted in each step of the chemical transformation. The SEM image (Figure 3a) shows that the $PbBr_2$ was well patterned after the photolithography process. The target size for each side of the $PbBr_2$ square pattern was 10 µm, and the pattern was formed with no overetching under optimized SDE conditions (SDE solvent: TMAH aqueous solution, 15 s; Rinsing solvent: DI, 1 s). Figure 3b,c shows the SEM images after reacting the $PbBr_2$ film array in CsBr solution for 10 and 30 min, respectively. After 10 min, there was no significant change in the square shape and pattern size, but small crystals with different contrasts were observed in several places. After 30 min, several crystals were formed. The overall size was similar, with each pattern consisting of crystals of various shapes with sizes ranging from 1 to 5 µm.

EDS mapping data of $PbBr_2$ (Figure 3d) indicate the existence of only Pb and Br, and no Cs. After the 10 min reaction, Cs diffusion occurred, and Cs was observed in the square pattern (Figure 3e). After the 30 min reaction, the vivid color of Cs was observed in the pattern (Figure 3f). Then, the quantitative element ratio was analyzed by SEM-EDS, as shown in Figure 3g. The EDS results show that the Cs: Pb: Br ratio after the 0, 10, and 30 min reaction is similar to that of $PbBr_2$, $CsPbBr_3$, and Cs_4PbBr_6, respectively (Figure S5 and Table S1, Supporting Information). Figure 3h and Figure S6 (Supporting Information) show the structural analysis via X-ray diffraction (XRD). $PbBr_2$ showed 2θ peaks of 18.7°, 41.1°, and 51.8°. After reacting with CsBr for 10 min, the $PbBr_2$ film showed 2θ peaks at ≈15.3°, 30.8°, 34.5°, 37.9°, 44.1°, and 49.6°. After reacting for 30 min, it showed 2θ peaks at ≈12.9°, 20.1°, 22.5°, 27.5°, and 28.6°. The XRD results after the reaction with CsBr for 0, 10, and 30 min are consistent with the values of $PbBr_2$, $CsPbBr_3$, and Cs_4PbBr_6 in the literature, respectively.[31] Through structural analysis, it was found that $Cs_xPb_yBr_z$ with different Cs ratios can be synthesized by controlling the reaction time of the $PbBr_2$ pattern with CsBr.

Figure 4 shows the optical properties of the $PbBr_2$ and $Cs_xPb_yBr_z$ films. The UV–vis spectra of the samples are shown in Figure 4a. In the graph, the $PbBr_2$ film without treatment with CsBr showed a peak at 328 nm, while $CsPbBr_3$ showed a large peak at 516 nm and other peaks at 365 and 315 nm. Cs_4PbBr_6 exhibited a small absorption peak at 515 nm and a large one at 308 nm (Figure S7, Supporting Information). The bandgap of each material was calculated through Tauc plot extrapolation, as shown in Figure 4b. The bandgaps of $PbBr_2$, $CsPbBr_3$, and Cs_4PbBr_6 are 3.57, 2.34, and 3.46 eV, respectively, which is consistent with previously reported values.[32] The photoluminescence (PL) spectra of the samples are shown in Figure 4c. $PbBr_2$ showed no PL peak, while $CsPbBr_3$ showed almost no PL peak. Cs_4PbBr_6 showed a strong PL peak at 517.8 nm, which is almost 100 times stronger than that of $CsPbBr_3$.

Several studies have reported that bulk $CsPbBr_3$ exhibits little PL, unlike $CsPbBr_3$ nanoparticles (NPs).[33,34] Owing to the nanoscale physical size of $CsPbBr_3$ NPs, the quantum confinement of charge carriers occurs.[35] Spatial constraint prevents electron and hole separation and induces recombination, resulting in a high PL. In bulk $CsPbBr_3$, quantum confinement does not occur, and electrons and holes are easily separated and/or trapped on the surface or in defects, leading to nonradiative recombination and low PL.[36] To investigate the PL mechanism in Cs_4PbBr_6, PL excitation (PLE) measurements with emission at 520 nm were conducted. Figure 4d shows the PLE, absorbance, and PL of Cs_4PbBr_6. The absorbance peak was at 308 nm; the PLE peaks were at 344 and 360.5 nm; and the PL peak was at 517.8 nm. The positions of the absorption peak and PL peak of Cs_4PbBr_6 have a difference of ≈210 nm, while that of the PLE peak and PL peak of Cs_4PbBr_6 is 160 nm. This large difference in absorbance and emission peaks indicates that the light absorbed by Cs_4PbBr_6 was emitted through states with a lower energy bandgap.

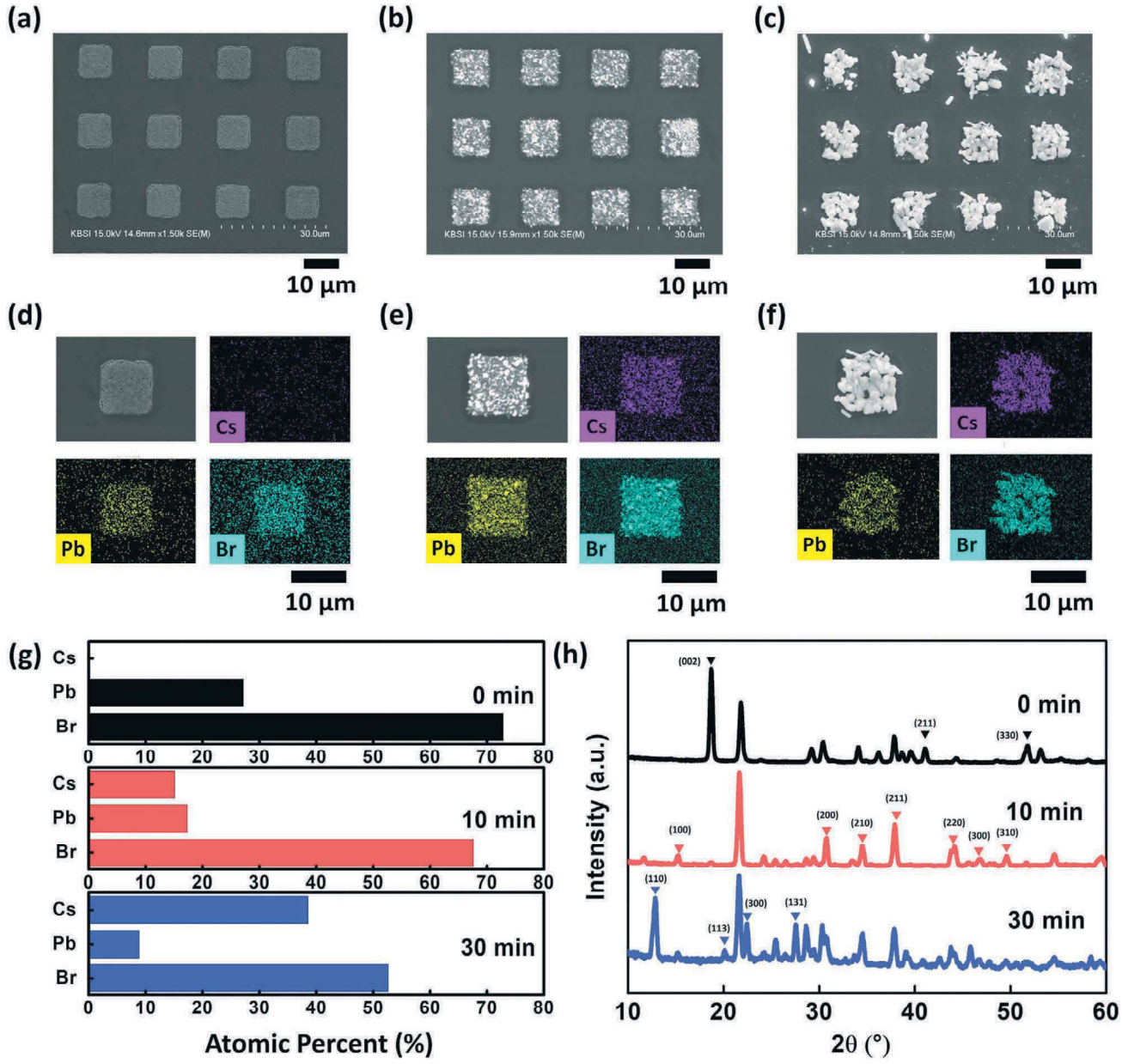

Figure 3. Measurement data after reacting the $PbBr_2$ pattern with CsBr solution for 0, 10, and 30 min. a–c) SEM image; d–f) SEM-EDS mapping of Cs, Pb, and Br; g) SEM-EDS elemental analysis; and h) XRD analysis: $PbBr_2$ peak (black), $CsPbBr_3$ peak (red), and Cs_4PbBr_6 peak (blue) (scale bar = 10 μm).

The unique PL mechanism of Cs_4PbBr_6 can be interpreted in two ways. First, $CsPbBr_3$ NPs are present in the Cs_4PbBr_6 matrix, which is the source of green light emission.[37–42] As quantum confinement occurs by the Cs_4PbBr_6 matrix around the nanoscale $CsPbBr_3$, it can exhibit high PL similar to $CsPbBr_3$ NPs. The small shoulder at 515 nm in the absorbance spectrum and strong emission at 517.8 nm supports the existence of $CsPbBr_3$ NPs and the emission through them. Second, light is emitted through the mid-bandgap state caused by the structural defects of Cs_4PbBr_6. It is known that bromide vacancy (V_{Br}), hydroxide (–OH) group or dislocation, such as planar slip, can induce mid-bandgap states.[43–45] Because the emission, PLE peak, and small absorption near 516 nm of the synthesized Cs_4PbBr_6 are similar to those reported for $CsPbBr_3$ NPs, we believe that the emission of Cs_4PbBr_6 originated from $CsPbBr_3$ NPs in the Cs_4PbBr_6 crystal matrix. However, further studies are needed to confirm the origin of PL in Cs_4PbBr_6. These optical analysis results indicate that $CsPbBr_3$ has good absorption performance, while Cs_4PbBr_6 exhibits excellent light emission performance. Thus, we confirmed that a phase favorable for light absorption and another favorable for light emission may be selectively synthesized by controlling the reaction time between the $PbBr_2$ film and CsBr solution.

The patterning method optimized in this study enables the high-resolution optoelectronic device applications of perovskite arrays. As a proof of concept, we fabricated optoelectronic and optical device arrays using high absorbance and high luminescence $CsPbBr_3$ and Cs_4PbBr_6, respectively. (**Figure 5**). A

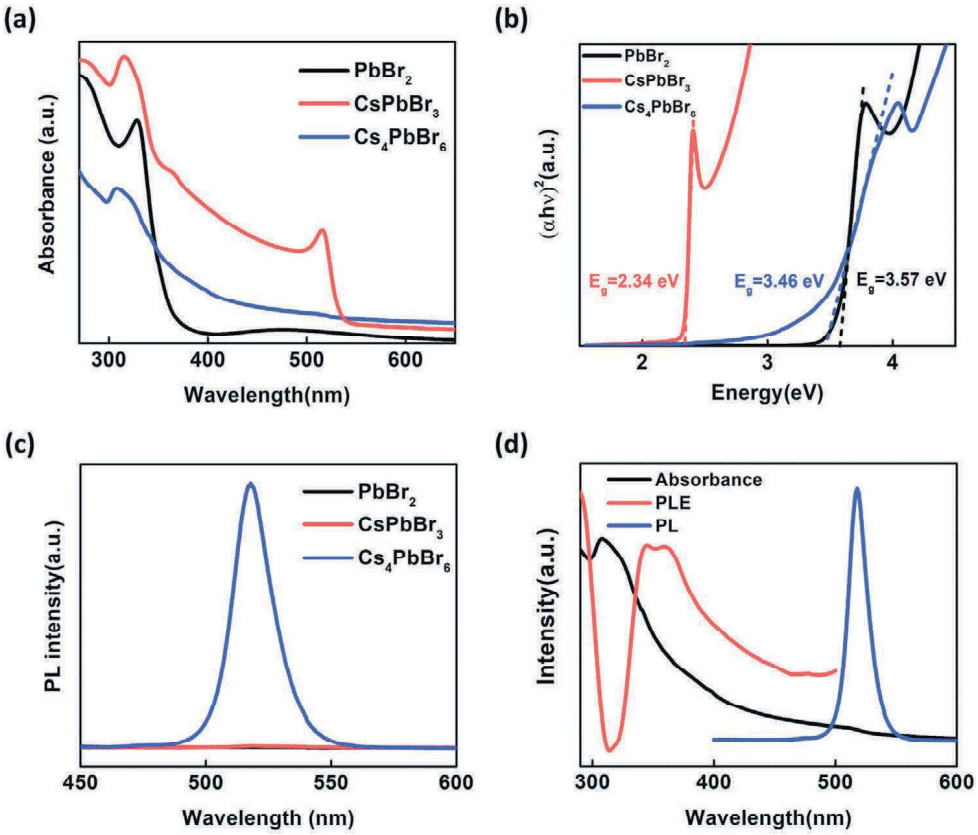

Figure 4. After the reaction of the $PbBr_2$ film with CsBr solution for 0, 10, 30 min: a) UV–vis data, b) Tauc plot extrapolation, and c) PL intensity data (λ_{ex} = 365 nm). d) Normalized absorbance, PL, and PL excitation of Cs_4PbBr_6 (λ_{em} = 520 nm).

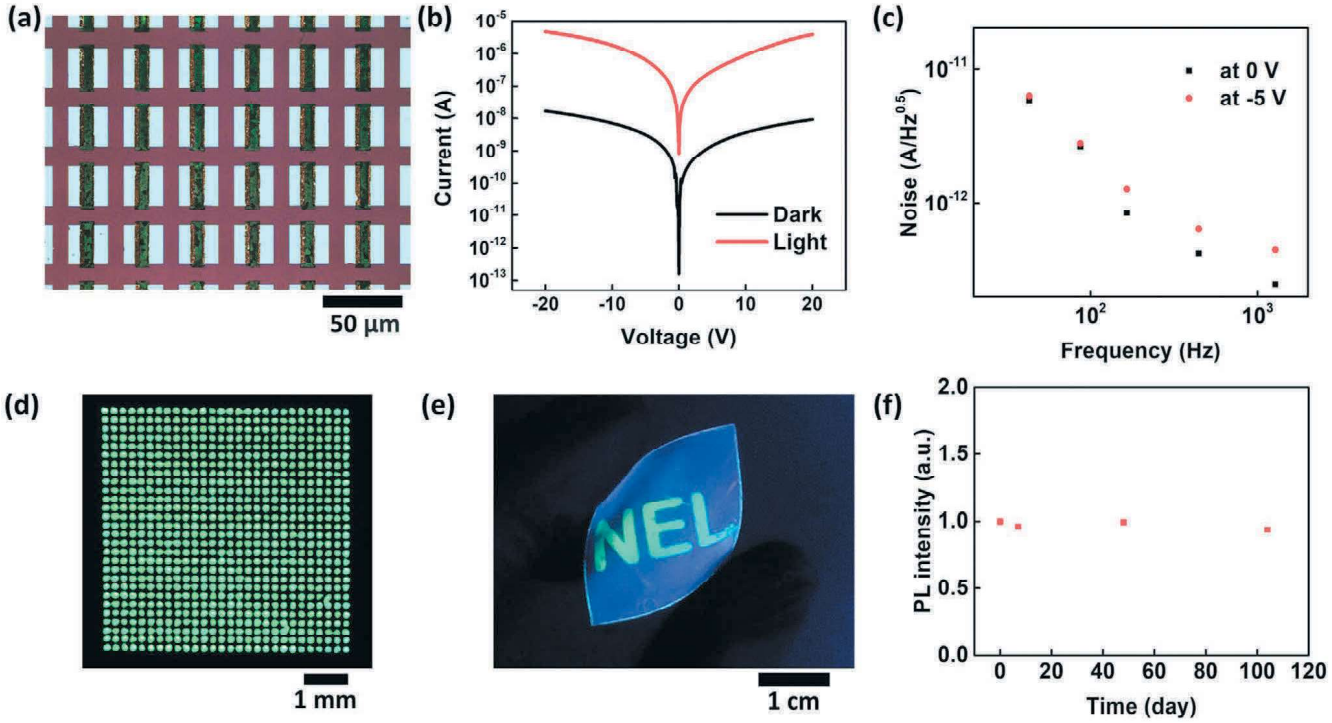

Figure 5. a) Optical image of $CsPbBr_3$ photoconductor array. b) Photoconductor ON and OFF *I–V* curve. c) Noise of photoconductor. d) PL image of Cs_4PbBr_6 array. e) Cs_4PbBr_6 PL image patterned on flexible substrate. f) Stability test of patterned Cs_4PbBr_6 at atmospheric condition.

patterned $CsPbBr_3$ array was fabricated for photoconductor applications in Figure 5a. A chromium-gold (Cr-Au) layer was used as the electrode, and $CsPbBr_3$ was patterned between the electrodes. The size of the $CsPbBr_3$ pattern was 10×30 μm^2, and 820 pixels are fabricated in 0.7×1.54 cm^2, corresponding to a density of 4915 pixels per square inch (Figure S8, Supporting Information). Figure 5b shows the *I*–*V* curves in darkness and illumination (525 nm, 2.55 mW cm^{-2}) of the $CsPbBr_3$ photoconductor array fabricated using an interdigital electrode with a device area of 4.5×10^{-2} cm^2 via a 10 min reaction in CsBr solution. The OFF (dark) current and ON (illuminated) current at 5 V are 1.44×10^{-9} and 2.90×10^{-7} A, respectively, with an ON/OFF ratio of 2.01×10^2 (Figure 5b). The device exhibits a low noise current of 7.11×10^{-13} A Hz$^{-0.5}$ at 0 V and 1.02×10^{-12}A Hz$^{-0.5}$ at −5 V at 300 Hz (Figure 5c). ON and OFF switching measurements were conducted for a constant laser light under 5 V. The constant optoelectronic performance after several cycles proves the reproducibility and stability of the fabricated photoconductor (Figure S9, Supporting Information).

The Cs_4PbBr_6 pattern was fabricated for potential optical applications such as color filters and displays. A Cs_4PbBr_6 array arranged in squares with a length and pitch of 100 μm was patterned via a 30 min reaction in CsBr solution. Under a 365 nm UV light, each square in the array emitted a bright green light (Figure 5d). A Cs_4PbBr_6 pattern was fabricated on a polyethylene terephthalate (PET) substrate (Figure 5e), which also emitted a bright green light under a 365 nm UV light. The constant PL intensity after several bending cycles indicates that the fabricated Cs_4PbBr_6 pattern has good adhesion to the PET substrate (Figure S10, Supporting Information). To confirm the stability of the patterned luminescent perovskite, the change in PL intensity over time was measured after fabrication, as shown in Figure 5f. After 100 days, the Cs_4PbBr_6 array maintained stable luminescence properties with no decrease in PL intensity under ambient enviorment. Thus, our optimized patterning technology can be applied to fabricate photoconductors and color filters on various substrates with very small perovskite patterns to obtain high-resolution optoelectronic device arrays without the degradation of optoelectronic performance (Figure S11, Supporting Information).

3. Conclusion

We propose a novel photolithography-based perovskite patterning method that enables high-resolution patterning and phase control to fabricate device arrays. Based on the chemical reaction and material analysis used in each process, a perovskite-compatible SDE and rinsing method was designed. Using our patterning method, photodetector arrays and luminescence patterns were demonstrated using $CsPbBr_3$ and Cs_4PbBr_6 pattern arrays. This study addressed the current challenge of patterning perovskite because of its vulnerability to chemicals and incompatibility with photolithography via a two-step process, and successfully fabricated optical and optoelectronic device arrays. We believe that our research will enable the development of perovskite optical and optoelectronic device array fabrication processes.

4. Experimental Section

Materials: Lead (II) bromide ($PbBr_2$, 99.9%), cesium bromide (CsBr, 99.9%), *N*,*N*-dimethylformamide (DMF, anhydrous, 99.8%), toluene (anhydrous, 99.8%), hexane (anhydrous, 95%), acetone (anhydrous, ≥99.5%), methyl alcohol (methanol, anhydrous, 99.8%), *iso*-propyl alcohol (IPA, anhydrous, 99.5%), AZ GXR 601 (46 cp), and MIF 300K (tetramethylammonium hydroxide (TMAH) aqueous solution) were purchased from Sigma-Aldrich. PET films (SKC). All reagents were used without further purification.

Preparation of $PbBr_2$ Film and CsBr Solution: Glass (or Si, PET) substrates were cleaned by sequential sonication for 20 min in warm deionized toluene, acetone, IPA, and water. After drying under a nitrogen flow at atmosphere, the substrates were treated with UV-ozone for 60 min and used immediately. $PbBr_2$ (367 mg) in 1 mL DMF was stirred on a hot plate at 90 °C for 3 h, filtered with a 0.22 μm pore size PTFE filter, and used immediately. The $PbBr_2$ layer was spin-coated at 4000 rpm for 30 s on this well-cleaned substrate and dried at 90 °C for 30 min. CsBr (25 mg) was dissolved in 1 mL methanol and heated to 50 °C for 1 h in a sealed container.

Patterning of $PbBr_2$ Film: PR was spin-coated at 4000 rpm for 30 s on the $PbBr_2$ film, and then annealed on a 90 °C hot plate for 60 s. Afterward, the film was selectively exposed to 365 nm UV light for 20 s by photomask and UV exposure (COOLUV-100), and then annealed on a 110 °C hot plate for 120 s. The pattern was developed by MIF-300Z for 15 s and then rinsed for 1 s with water. After substrate drying by nitrogen flow, the unexposed PR was lifted off by acetone to produce the $PbBr_2$ pattern.

Converting $PbBr_2$ Film into $Cs_xPb_yBr_z$: The substrate was immersed in a heated (50 °C) 25 mg mL^{-1} CsBr solution in a sealed container for 10–30 min. Then, it was taken out and rinsed by pouring −20 °C IPA and annealed on a 180 °C hot plate for 10 min.

Characterization: The optical properties were analyzed by ultraviolet–vis (UV–vis) spectroscopy (Cary 5000, Agilent Technologies) and PL spectroscopy (FP-8500, JASCO). The structural properties were measured by XRD (MAX-2500V, Rigaku), scanning electron microscopy energy-dispersive X-ray spectroscopy (SEM-EDS, Model Hitachi S-4300, Hitachi High Technologies America, Inc.), and an optical microscope (MA200, Nikon). The surface depth profile was measured by an alpha-step profilometer (ET200, Kosaka Laboratory Ltd.). A probe station (Model MST-4000A, MSTECH) was utilized to measure the current of the $CsPbBr_3$ photoconductor. The detector dark current was amplified by a low-noise current amplifier (SR 570, Stanford Research Systems) and then recorded by a lock-in (SR 530, Stanford Research Systems) amplifier. The bias on the device was provided by the low-noise current amplifier, while the set frequency was from the external clock of the lock-in amplifier.

Supporting Information

Supporting Information is available from the Wiley Online Library or from the author.

Acknowledgements

This research was supported by the Creative Materials Discovery Program through the National Research Foundation of Korea (NRF) funded by Ministry of Science and ICT (NRF-2018M3D1A1059001), the Basic Science Research Program through the National Research Foundation of Korea (NRF), funded by the Ministry of Science, ICT and Future Planning (2019R1C1C1003319), the National Research Foundation of Korea (NRF) funded by the Material Innovation Project (NRF-2021M3H4A3026733, NRF-2020M3H4A3081791), Korea Institute for Advancement of Technology (KIAT) grant funded by the Korea Government (MOTIE) (P0002019, Human Resource Development Program for Industrial Innovation).

Conflict of Interest

The authors declare no conflict of interest.

Data Availability Statement

The data that support the findings of this study are available in the supplementary material of this article.

Keywords

device arrays, lithography, patterning, perovskites

Received: November 9, 2021
Revised: December 11, 2021
Published online: January 3, 2022

[1] J. Liang, J. Liu, Z. Jin, *Sol. RRL* **2017**, *1*, 1700086.
[2] M. V. Kovalenko, L. Protesescu, M. I. Bodnarchuk, *Science* **2017**, *358*, 745.
[3] G. Nedelcu, L. Protesescu, S. Yakunin, M. I. Bodnarchuk, M. J. Grotevent, M. v. Kovalenko, *Nano Lett.* **2015**, *15*, 5635.
[4] J. Feng, X. Han, H. Huang, Q. Meng, Z. Zhu, T. Yu, Z. Li, Z. Zou, *Sci. Bull.* **2020**, *65*, 726.
[5] Q. Chen, H. Zhou, Z. Hong, S. Luo, H. S. Duan, H. H. Wang, Y. Liu, G. Li, Y. Yang, *J. Am. Chem. Soc.* **2014**, *136*, 622.
[6] H. Mehdi, A. Mhamdi, R. Hannachi, A. Bouazizi, *RSC Adv.* **2019**, *9*, 12906.
[7] X. Zheng, S. Yuan, J. Liu, J. Yin, F. Yuan, W. S. Shen, K. Yao, M. Wei, C. Zhou, K. Song, B. B. Zhang, Y. Lin, M. N. Hedhili, N. Wehbe, Y. Han, H. T. Sun, Z. H. Lu, T. D. Anthopoulos, O. F. Mohammed, E. H. Sargent, L. S. Liao, O. M. Bakr, *ACS Energy Lett.* **2020**, *5*, 793.
[8] J. Chang, S. Zhang, N. Wang, Y. Sun, Y. Wei, R. Li, C. Yi, J. Wang, W. Huang, *J. Phys. Chem. Lett.* **2018**, *9*, 881.
[9] M. Yuan, L. N. Quan, R. Comin, G. Walters, R. Sabatini, O. Voznyy, S. Hoogland, Y. Zhao, E. M. Beauregard, P. Kanjanaboos, Z. Lu, D. H. Kim, E. H. Sargent, *Nat. Nanotechnol.* **2016**, *11*, 872.
[10] Y. H. Kim, S. Kim, A. Kakekhani, J. Park, J. Park, Y. H. Lee, H. Xu, S. Nagane, R. B. Wexler, D. H. Kim, S. H. Jo, L. Martínez-Sarti, P. Tan, A. Sadhanala, G. S. Park, Y. W. Kim, B. Hu, H. J. Bolink, S. Yoo, R. H. Friend, A. M. Rappe, T. W. Lee, *Nat. Photonics* **2021**, *15*, 148.
[11] D. Liu, Z. Hu, W. Hu, P. Wangyang, K. Yu, M. Wen, Z. Zu, J. Liu, M. Wang, W. Chen, M. Zhou, X. Tang, Z. Zang, *Mater. Lett.* **2017**, *186*, 243.
[12] J. Gao, Q. Liang, G. Li, T. Ji, Y. Liu, M. Fan, Y. Hao, S. F. Liu, Y. Wu, Y. Cui, *J. Mater. Chem. C* **2019**, *7*, 8357.
[13] P. Ramasamy, D. H. Lim, B. Kim, S. H. Lee, M. S. Lee, J. S. Lee, *Chem. Commun.* **2016**, *52*, 2067.
[14] J. Chen, N. G. Park, *J. Phys. Chem. C* **2018**, *122*, 14039.
[15] Z. Fan, K. Sun, J. Wang, *J. Mater. Chem. A* **2015**, *3*, 18809.
[16] J. Burschka, N. Pellet, S. J. Moon, R. Humphry-Baker, P. Gao, M. K. Nazeeruddin, M. Grätzel, *Nature* **2013**, *499*, 316.
[17] H. Rao, S. Ye, F. Gu, Z. Zhao, Z. Liu, Z. Bian, C. Huang, *Adv. Energy Mater.* **2018**, *8*, 1800758.
[18] X. Du, G. Wu, J. Cheng, H. Dang, K. Ma, Y. W. Zhang, P. F. Tan, S. Chen, *RSC Adv.* **2017**, *7*, 10391.
[19] J. Harwell, J. Burch, A. Fikouras, M. C. Gather, A. di Falco, I. D. W. Samuel, *ACS Nano* **2019**, *13*, 3823.
[20] R. Chen, Z. Liang, W. Feng, X. Hu, A. Hao, *J. Alloys Compd.* **2021**, *864*, 158125.
[21] C. K. Lin, Q. Zhao, Y. Zhang, S. Cestellos-Blanco, Q. Kong, M. Lai, J. Kang, P. Yang, *ACS Nano* **2020**, *14*, 3500.
[22] W. Lee, J. Lee, H. Yun, J. Kim, J. Park, C. Choi, D. C. Kim, H. Seo, H. Lee, J. W. Yu, W. B. Lee, D. H. Kim, *Adv. Mater.* **2017**, *29*, 1702902.
[23] H. Du, K. Wang, L. Zhao, C. Xue, M. Zhang, W. Wen, G. Xing, J. Wu, *ACS Appl. Mater. Interfaces* **2020**, *12*, 2662.
[24] G. Kim, S. An, S. K. Hyeong, S. K. Lee, M. Kim, N. Shin, *Chem. Mater.* **2019**, *31*, 8212.
[25] J. Liu, L. Zhu, S. Xiang, Y. Wei, M. Xie, H. Liu, W. Li, H. Chen, *Sustainable Energy Fuels* **2019**, *3*, 184.
[26] J. H. Cha, J. H. Han, W. Yin, C. Park, Y. Park, T. K. Ahn, J. H. Cho, D. Y. Jung, *J. Phys. Chem. Lett.* **2017**, *8*, 565.
[27] D. Barrit, P. Cheng, K. Darabi, M.-C. Tang, D.-M. Smilgies, S. (F.) Liu, T. D. Anthopoulos, K. Zhao, A. Amassian, *Adv. Funct. Mater.* **2020**, *30*, 1907442.
[28] P. Teng, X. Han, J. Li, Y. Xu, L. Kang, Y. Wang, Y. Yang, T. Yu, *ACS Appl. Mater. Interfaces* **2018**, *10*, 9541.
[29] J. Liu, L. Zhu, S. Xiang, Y. Wei, M. Xie, H. Liu, W. Li, H. Chen, *Sustainable Energy Fuels* **2019**, *3*, 184.
[30] K. C. Tang, P. You, F. Yan, *Sol. RRL* **2018**, *2*, 1800075.
[31] X. Peng, J. Chen, F. Wang, C. Zhang, B. Yang, *Optik* **2020**, *208*, 164579.
[32] J. Yin, P. Maity, M. de Bastiani, I. Dursun, O. M. Bakr, J. L. Brédas, O. F. Mohammed, *Sci. Adv.* **2017**, *3*, 1701793.
[33] J. Li, H. Zhang, S. Wang, D. Long, M. Li, D. Wang, T. Zhang, *Materials* **2018**, *11*, 778.
[34] J. Bao, V. G. Hadjiev, *Nano-Micro Lett.* **2019**, *11*, 26.
[35] Y. Jiang, B. Li, T. Zhang, Y. Shi, Q. H. Xu, *ChemNanoMat* **2020**, *6*, 327.
[36] H. Baker, D. Strandell, P. Kambhampati, *J. Phys. Chem. C* **2020**, *124*, 18816.
[37] T. Xuan, S. Lou, J. Huang, L. Cao, X. Yang, H. Li, J. Wang, *Nanoscale* **2018**, *10*, 9840.
[38] S. Cho, S. H. Yun, *Commun. Chem.* **2020**, *3*, 15.
[39] S. Lou, T. Xuan, Q. Liang, J. Huang, L. Cao, C. Yu, M. Cao, C. Xia, J. Wang, D. Zhang, H. Li, *J. Colloid Interface Sci.* **2019**, *537*, 384.
[40] L. Xu, J. Li, T. Fang, Y. Zhao, S. Yuan, Y. Dong, J. Song, *Nanoscale Adv.* **2019**, *1*, 980.
[41] Q. A. Akkerman, S. Park, E. Radicchi, F. Nunzi, E. Mosconi, F. de Angelis, R. Brescia, P. Rastogi, M. Prato, L. Manna, *Nano Lett.* **2017**, *17*, 1924.
[42] W. Wang, Y. Wu, D. Wang, T. Zhang, *ACS Omega* **2019**, *4*, 19641.
[43] M. de Bastiani, I. Dursun, Y. Zhang, B. A. Alshankiti, X. H. Miao, J. Yin, E. Yengel, E. Alarousu, B. Turedi, J. M. Almutlaq, M. I. Saidaminov, S. Mitra, I. Gereige, A. Alsaggaf, Y. Zhu, Y. Han, I. S. Roqan, J. L. Bredas, O. F. Mohammed, O. M. Bakr, *Chem. Mater.* **2017**, *29*, 7108.
[44] A. Ray, D. Maggioni, D. Baranov, Z. Dang, M. Prato, Q. A. Akkerman, L. Goldoni, E. Caneva, L. Manna, A. L. Abdelhady, *Chem. Mater.* **2019**, *31*, 7761.
[45] R. Sun, N. Liu, W. Zheng, J. Zhang, N. Li, H. Lian, H. Liu, Y. Zhang, *Chem. Mater.* **2021**, *33*, 3721.